Fermilab Library
0 1160 0041403 1

UNIVERSITY OF DURHAM

Centre For Particle Theory

DTP-95/18

February, 1995

What we can learn by measuring $\gamma\gamma \to \pi\pi$ at DAΦNE

M.R. Pennington

Centre for Particle Theory,
University of Durham
Durham DH1 3LE, U.K.

FERMILAB
APR 10 1995
LIBRARY

To be published in the Second DAΦNE Physics Handbook, eds.
L. Maiani, G. Pancheri and N. Paver

What we learn by measuring $\gamma\gamma \to \pi\pi$ at DAΦNE

M.R. Pennington

Centre for Particle Theory, University of Durham,

Durham DH1 3LE, U.K.

Dispersion relations provide a framework for the model-independent determination of key parameters of hadron dynamics from measurements of $\gamma\gamma \to \pi\pi$ scattering. This framework is outlined. Particular attention is paid to the range of applicability of approximations made in practical calculations and the consequent uncertainty in predictions or quantities extracted. Precise measurements at DAΦNE of the reactions $\gamma\gamma \to \pi^+\pi^-$ and $\pi^0\pi^0$ at low energies over as complete an angular coverage as possible will impose constraints on $\pi\pi$ phases, test Chiral Perturbation Theory and provide a firmer basis for the determination of two photon couplings of the $I = 0$ scalar resonances at higher $\pi\pi$ masses and so help to solve the enigma of their structure.

1. Introduction

At low energy the cross-section, integrated and differential, for the reaction $\gamma\gamma \to \pi\pi$, Fig. 1, observed in $e^+e^- \to e^+e^-\pi\pi$ [1], can be computed exactly with minimal assumptions. This makes this reaction almost unique among processes in which important strong interaction effects occur.

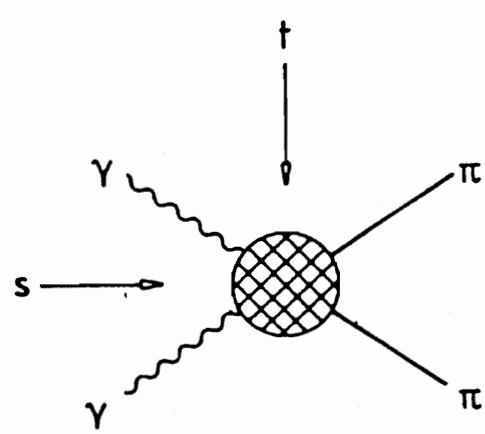

Figure 1: The process $\gamma\gamma \to \pi\pi$ in the s-channel.

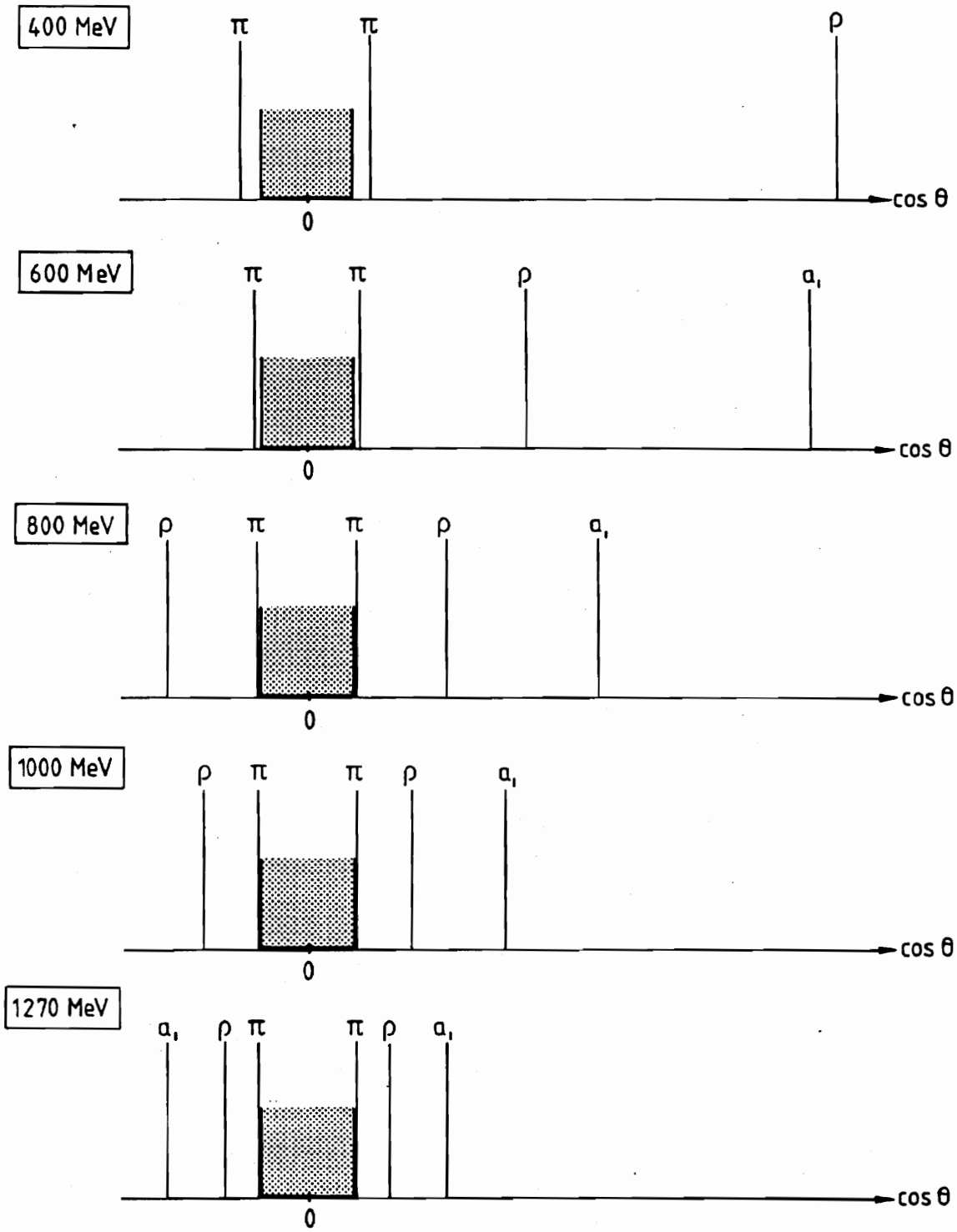

Figure 3: Nearness of poles in the t & u-channels ($\gamma\pi \to \gamma\pi$) from π, ρ and a_1-exchange to the s-channel ($\gamma\gamma \to \pi\pi$) physical region, $-1 \leq \cos\theta \leq 1$, depicted as the shaded region, at different $\pi\pi$ masses.

isospin components.

The photons scatter with either their helicities parallel or anti-parallel, so the observables are specified by two helicity amplitudes [1] $\mathcal{M}^{c,n}_{++}$ and $\mathcal{M}^{c,n}_{+-}$, where c denotes charged pion production and n neutral. With unpolarised beams one only measures the sum of the squares of the moduli of these amplitudes, so at a $\gamma\gamma$ c.m. energy of $\sqrt{s}$ the differential cross-sections are :

$$\frac{d\sigma^{c,n}}{d\Omega} = \frac{\beta}{128\pi^2 s}\left[\mid \mathcal{M}^{c,n}_{++} \mid^2 + \mid \mathcal{M}^{c,n}_{+-} \mid^2\right] \tag{1}$$

where $\beta = \sqrt{1-4m_\pi^2/s}$ with m_π appropriately the charged or neutral pion mass. The helicity amplitudes can be partial wave projected to give the components, $\mathcal{F}^{c,n}_{J,\lambda}(s)$, with $\pi\pi$ spin J and helicity λ (=0 or 2) with even $J \geq \lambda$, defined by :

$$\begin{aligned} \mathcal{M}^{c,n}_{++}(s,\theta,\phi) &= e^2\sqrt{16\pi}\sum_{J\geq 0}\mathcal{F}^{c,n}_{J0}(s)\,Y_{J0}(\theta,\phi) \\ \mathcal{M}^{c,n}_{+-}(s,\theta,\phi) &= e^2\sqrt{16\pi}\sum_{J\geq 2}\mathcal{F}^{c,n}_{J2}(s)\,Y_{J2}(\theta,\phi) \end{aligned} \tag{2}$$

where the factor of $e^2\sqrt{16\pi}$ has been taken out for later convenience. With this normalization the integrated cross-sections are

$$\sigma^{c,n} = 2\pi\alpha^2\frac{\beta}{s}\sum_{J\geq\lambda}\mid \mathcal{F}^{c,n}_{J\lambda} \mid^2 . \tag{3}$$

These amplitudes and their partial waves are combinations of amplitudes with definite $\pi\pi$ isospin I, $\mathcal{F}^I$, in terms of which the amplitudes for the physical processes $\gamma\gamma \to \pi^+\pi^-$ and $\gamma\gamma \to \pi^0\pi^0$ are [2] :

$$\mathcal{F}^c = \sqrt{\frac{2}{3}}\mathcal{F}^0 + \sqrt{\frac{1}{3}}\mathcal{F}^2 \quad ; \quad \mathcal{F}^n = -\sqrt{\frac{1}{3}}\mathcal{F}^0 + \sqrt{\frac{2}{3}}\mathcal{F}^2 \quad . \tag{4}$$

Note once more that the one-pion exchange Born term contributes to both isospin amplitudes.

[2] the sign of the amplitudes is a matter of convention; some others use the opposite sign for the neutral one.

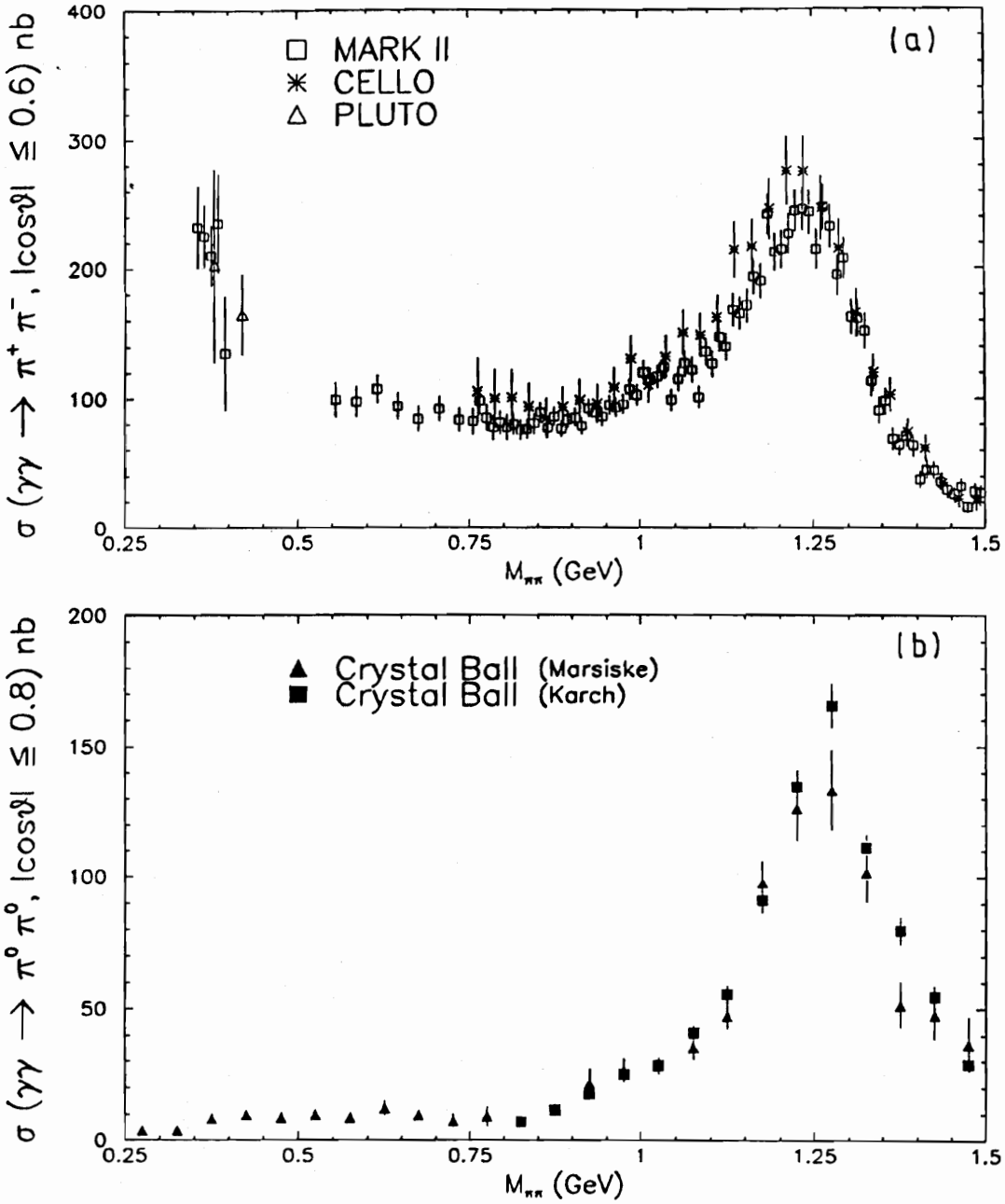

Figure 4: (a) $\gamma\gamma \to \pi^+\pi^-$ cross-section for $|\cos\theta| \leq 0.6$ from Mark II [7] , CELLO [8] and PLUTO [9] — the last of these is only shown at low $\pi\pi$ mass where the experimental results on $d\sigma/d|\cos\theta|$ at $\cos\theta = 0$ can be scaled to give σ for $|\cos\theta| \leq 0.6$ assuming a flat distribution ; (b) $\gamma\gamma \to \pi^0\pi^0$ cross-section for $|\cos\theta| \leq 0.8$ from Crystal Ball [10] (labelled Marsiske) and the higher statistics, higher mass data (labelled Karch) tabulated in the data review by Morgan et al. [1].
Both are as functions of $\pi\pi$ invariant mass.

2. The Dispersive Approach

Let us discuss the properties of the partial wave amplitudes, $\mathcal{F}^I_{J,\lambda}(s)$, and what we need to know to calculate them [13, 14, 3, 4]. Firstly, these amplitudes are analytic functions of s. They have a left hand cut starting at $s = 0$ from the pion exchange Born term and then other cuts running to the left from $s = -(M^2 - m_\pi^2)^2/M^2$ generated by ρ, ω and other exchanges of mass M. Of course, only the nearby part of the left hand cut from $s = 0$ to $s = -m^2_{\rho,\omega}$ is really known from one pion exchange [3]. For $s \lesssim -m^2_{\rho,\omega}$, form-factor damping in the $\gamma V \pi$ vertex (where $V = \rho$ or ω) as well as other exchanges affect the left hand cut discontinuity.

The partial wave amplitudes also have a right hand cut generated by final state interactions. At low energy, the only possible strong interaction is $\gamma\gamma \to \pi\pi$. Then the final state pions will scatter strongly back to $\pi\pi$. Indeed, it is in this way that the cross-section for $\gamma\gamma \to \pi^0\pi^0$ can readily become non-zero : $\gamma\gamma \to \pi^+\pi^- \to \pi^0\pi^0$, where the first process in the chain can occur by the Born term. Fortunately, such effects are exactly calculable, thanks to two body unitarity. Above inelastic threshold, which effectively means above $K\overline{K}$ threshold near 1 GeV, $\gamma\gamma$ can also go to K^+K^- , which in turn can scatter back to $\pi\pi$. Though unitarity still constrains these contributions, one needs information on $\gamma\gamma \to K\overline{K}$ and $\pi\pi \to K\overline{K}$ scattering, as well as $\pi\pi \to \pi\pi$, to know how. This means it is more difficult to implement the constraints of unitarity when many channels enter. However below roughly 1 GeV, elastic unitarity enforces Watson's theorem [15] that makes the phase of the partial waves for $\gamma\gamma \to \pi\pi$ for each I and J, $\mathcal{F}^I_{J,\lambda}(s)$, equal to the phase of the corresponding $\pi\pi \to \pi\pi$ amplitude, $\mathcal{T}^I_J(s)$. This is exceedingly useful, since knowledge of the phase of an amplitude largely determines the behaviour of its modulus — amplitudes being analytic functions. A simple example of this is the phase rising rapidly from 0° to 180°. The modulus then has to peak at a position and width wholly correlated with the phase variation. This relationship is exemplified by the well-known Breit-Wigner formula. The general relation between the phase and the modulus of the amplitude is embodied in the Omnès representation [16]. Thus knowing the phase of a partial wave amplitude, $\phi^I_{J,\lambda}$, from $\pi\pi$ threshold to infinity, we can define a function $\Omega^I_{J,\lambda}(s)$ (the Omnès function)

$$\Omega^I_{J,\lambda}(s) = |\,\Omega^I_{J,\lambda}(s)\,|\; e^{i\phi^I_{J,\lambda}(s)} = \exp\left[\frac{s}{\pi}\int_{4m_\pi^2}^{\infty} ds'\,\frac{\phi^I_{J,\lambda}(s')}{s'(s'-s)}\right] \quad , \tag{5}$$

where in the region of elastic unitarity $\phi^I_{J,\lambda}(s) = \delta^I_J(s)$, the $\pi\pi$ phase shift, independent of the two photon helicity λ. This function, Ω, has the phase ϕ by construction. The

way convergent dispersion relations work, Ω at low energies fortunately does not require detailed knowledge of the phase ϕ above 1 GeV. We will return to this later.

How this information can be used to compute $\gamma\gamma \to \pi\pi$ scattering is explained in detail in Ref. 6. Here we sketch the methodology. We can write an appropriately subtracted dispersion relation for each partial wave amplitude, specified by I, J and λ. For the S-waves ($J = 0$, $\lambda = 0$), these are twice subtracted [17] : two subtractions to suppress the dependence at low energies on what the *distant* left and right hand cut discontinuites are. That is, there should be only a weak dependence on both higher mass cross-channel exchanges and the phases of the $\gamma\gamma \to \pi\pi$ amplitudes above 1 GeV. The lack of knowledge of these terms is parametrized by two subtraction constants that are fixed by two crucial low energy constraints. Firstly, Low's theorem that states each partial wave amplitude equals its corresponding Born term at $s = 0$ — that follows from QED gauge invariance. Secondly, from chiral dynamics we have a prediction in the low energy region for the amplitude minus its Born term. Thus, for instance the neutral channel S-wave has a zero at $s = O(m_\pi^2)$ — in one loop Chiral Perturbation Theory (χPT) [18, 19] this is at $s_n = m_\pi^2$. In general, all we know is that these near threshold corrections are $O(m_\pi^2/f_\pi^2)$. These low energy limits fix the two subtraction constants, d_I, in the $I = 0$ and 2 $\gamma\gamma \to \pi\pi$ S-wave amplitudes. Thus

$$\mathcal{F}^I_{00}(s) \;=\; \mathcal{H}^I_{00}(s) \,+\, d_I s\, \Omega^I_{00}(s) \;-\; \frac{s^2 \Omega^I_{00}(s)}{\pi} \int_{4m_\pi^2}^{\infty} ds' \, \frac{\mathcal{H}^I_{00}(s')\, \mathrm{Im}(\Omega^I_{00}(s')^{-1})}{s'^2\,(s'-s)} \quad . \tag{6}$$

The functions $\mathcal{H}^I(s)$ have the complete left hand cut and no right hand cut. They are given by

$$\begin{aligned} \mathcal{H}^0(s) &= \sqrt{\frac{2}{3}}\,\mathcal{B}^\pi(s) - \mathcal{L}^\rho(s) - \sqrt{\frac{1}{3}}\,\mathcal{L}^\omega(s) \\ \mathcal{H}^2(s) &= \sqrt{\frac{1}{3}}\,\mathcal{B}^\pi(s) + \sqrt{\frac{2}{3}}\,\mathcal{L}^\omega(s) \quad , \end{aligned} \tag{7}$$

where $\mathcal{B}^\pi$ is the one pion exchange Born term and $\mathcal{L}^\rho$, $\mathcal{L}^\omega$ denote the contributions to the left-hand cut generated by exchanges with ρ and ω quantum numbers, respectively. Then the combinations in the charged and neutral channels are :

$$\begin{aligned} \mathcal{H}^c(s) &= \mathcal{B}^\pi(s) - \sqrt{\frac{2}{3}}\,\mathcal{L}^\rho(s) \\ \mathcal{H}^n(s) &= \sqrt{\frac{1}{3}}\,\mathcal{L}^\rho(s) + \mathcal{L}^\omega(s) \quad . \end{aligned} \tag{8}$$

According to Low's theorem : $\mathcal{H}^c \to \mathcal{B}^\pi$ and $\mathcal{H}^n \to 0$ as $s \to 0$, so in turn this means : $\mathcal{L}^\rho(s) \to 0$, $\mathcal{L}^\omega(s) \to 0$ as $s \to 0$. Recalling $\beta = \sqrt{1 - 4m_\pi^2/s}$ (Eq. (1)), the S-wave Born amplitude is, for example, [1, 3]

$$\mathcal{B}^\pi_{00}(s) = \frac{1-\beta^2}{2\beta} \ln\left(\frac{1+\beta}{1-\beta}\right) \tag{9}$$

with a cut for $s < 0$.

The fixing of subtraction constants by appeal to chiral dynamics only affects the S-wave amplitudes. The higher partial waves satisfy essentially once subtracted dispersion relations on dividing out their known threshold behaviour, so that only Low's QED theorem is needed for these waves. Thus [3]

$$\mathcal{F}^I_{J\lambda}(s) = \mathcal{H}^I_{J\lambda}(s) - \frac{s(s-4m_\pi^2)^{J/2}\,\Omega^I_{J\lambda}(s)}{\pi} \int_{4m_\pi^2}^{\infty} ds' \frac{\mathcal{H}^I_{J\lambda}(s')\,\mathrm{Im}(\Omega^I_{J\lambda}(s')^{-1})}{s'(s-4m_\pi^2)^{J/2}\,(s'-s)} \tag{10}$$

where the $\mathcal{H}^I_{J,\lambda}(s)$ are the appropriate partial waves of the left hand cut components of Eq. (8). Using Eqs. (3, 5-10), the cross-sections can then be deduced from these partial wave amplitudes.

It is useful for our later discussion, though not necessary for our low energy calculations, to note that these partial wave amplitudes , for all J, can be expressed quite generally [3] as :

$$\mathcal{F}^I_{J\lambda}(s) = \mathcal{P}^I_{J\lambda}(s)\,\mathcal{H}^I_{J\lambda}(s)\,\Omega^I_{J\lambda}(s) \quad , \tag{11}$$

where the function $\mathcal{H}^I_{J,\lambda}(s)$ has the left hand cut, Eq. (8), and $\Omega^I_{J,\lambda}(s)$ the right hand cut, Eq. (5), and $\mathcal{P}^I_{J,\lambda}(s)$ is a real polynomial. While $\mathcal{H}^I_{J,\lambda}(s)$ is the full left hand cut function, it is often convenient to model this function by some $h^I_{J,\lambda}$ (for instance, the Born term) and rewrite Eq. (11) as

$$\mathcal{F}^I_{J\lambda}(s) = \mathcal{P}_B(s)\,h^I_{J\lambda}(s)\,\Omega^I_{J\lambda}(s) + \mathcal{P}_C(s)\,\Omega^I_{J\lambda}(s) \ . \tag{12}$$

$\mathcal{P}_B$ and $\mathcal{P}_C$ (with I, J, λ labels suppressed) may now be more complicated functions along the left hand cut, but they will continue to be smooth along the right hand cut away from their singularities. In physical terms, the first term models the simple well understood cross-channel exchanges and then $\mathcal{P}_C(s)$ incorporates the *rest* as direct channel contributions. Near $\pi\pi$ threshold, $h^I_{J,\lambda}$ is just the pion exchange Born term and there are essentially no direct channel effects other than those of final state interactions automatically included in Eqs. (11,12). There

$$\mathcal{F}^I_{J\lambda}(s) \simeq \mathcal{P}_B(s)\,\mathcal{B}^\pi_{J\lambda}(s)\,\Omega^I_{J\lambda}(s) \tag{13}$$

to a good approximation. It is this fact that allows the low energy cross-section to be accurately predicted as we discuss in the next section.

One can go to slightly higher $\pi\pi$ masses, 500 MeV or so, by taking

$$h^I(s) = \mathcal{B}^\pi(s) + \mathcal{L}^{V=\rho,\omega}(s) \tag{14}$$

in Eq. (12) with $\mathcal{P}_C$ still zero. However, above that energy, direct channel effects (or equivalently heavier mass cross-channel exchanges) become increasingly important and definite predictions possible near threshold must give way to fitting data [3, 4, 11]. This is necessary to determine the form of $\mathcal{P}_C(s)$ and hence the direct channel couplings.

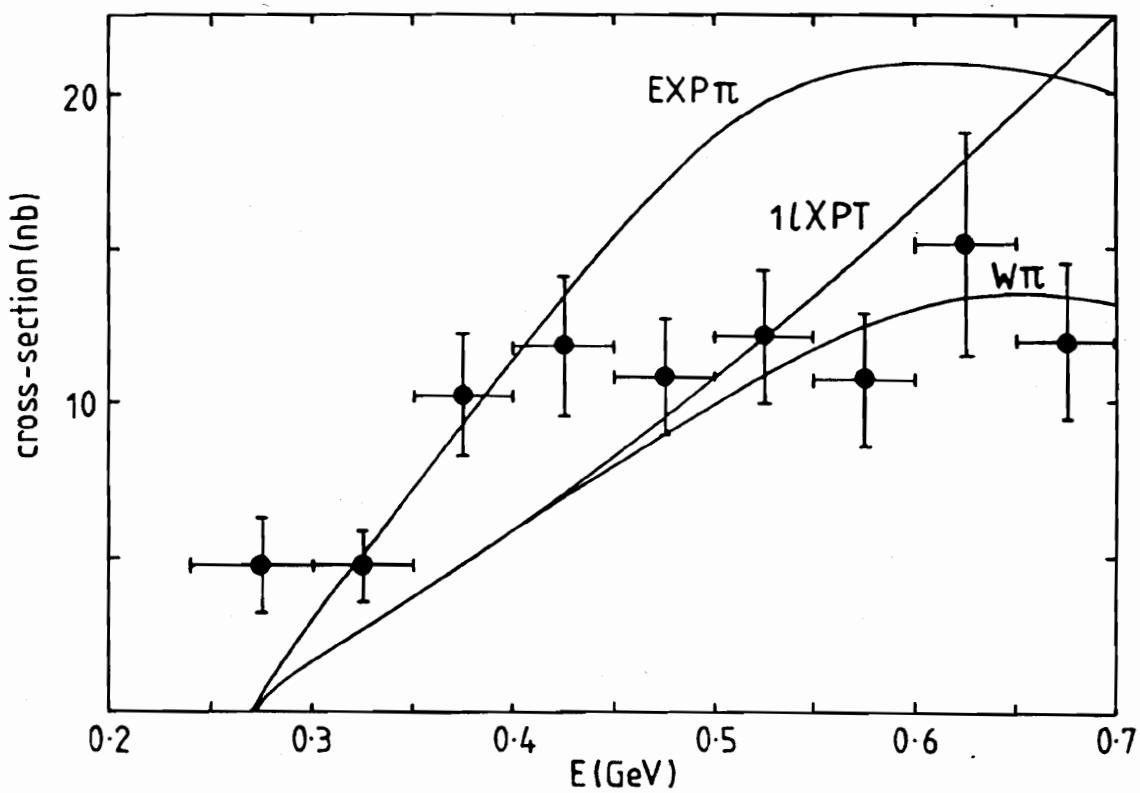

Figure 5: Integrated cross-section for $\gamma\gamma \to \pi^0\pi^0$ as a function of the $\pi\pi$ invariant mass, $E = \sqrt{s}$. The data are from Crystal Ball [3] scaled to the full angular range by a factor of 1.25. The line marked $1\ell\chi PT$ is the prediction of one loop Chiral Perturbation Theory [18, 19]. The curve marked "$W\pi$" is the dispersive calculation using Weinberg phases [20], while that labelled "$EXP\pi$" are the predictions from experimental $\pi\pi$ phases as described in [6] — both with just π-exchange for the left hand cut.

3. Dispersive Predictions

At low energies we can evaluate the dispersion relations for the S and higher waves, Eqs. (6,10). We input

(i) the phases of the $\pi\pi$ partial wave amplitude from $M_{\pi\pi} = 2m_\pi$ to 800 or 900 MeV (above that the phases are irrelevant for the $\gamma\gamma \to \pi\pi$ cross-section at low energies),

(ii) the discontinuity of the left hand cut — π-exchange plus whatever,

(iii) the slope of the $\gamma\gamma \to \pi\pi$ S-wave amplitudes minus their Born components in the sub-threshold region needed to fix the subtraction constants, d_I, in Eq. (6).

For orientation, we first perform a model calculation. We input

(i) the phases of Weinberg's model of $\pi\pi$ scattering [20],

(ii) assume only π-exchange in the crossed channels, and

(iii) we fix the slopes at $s = m_\pi^2$ from one loop χPT [18, 19] as there the neutral S-wave vanishes, i.e. $s_n = m_\pi^2$.

We turn the handle of the machinery defined in Eqs. (3-10,13,14) and out comes the cross-section for $\gamma\gamma \to \pi^0\pi^0$ marked "$W\pi$" shown in Fig. 5. Near threshold this is identical with the one loop calculation of this process in χPT by Bijnens and Cornet and by Donoghue, Holstein and Lin [18, 19]. Both the lines "$W\pi$" and "$1\ell\chi$PT" exhibit the much discussed disagreement with the near threshold data of Crystal Ball [10]. Above 500 MeV, the dispersive result flattens out, as it has to from unitarity, unlike one loop χPT . This calculation, which is here wholly numerical, has also been performed semi-analytically by Donoghue and Holstein [21], who simplify this exercise by setting $\mid \Omega_0^I(s) \mid \cos\delta_0^I = 1$ so that $\mathrm{Im}[\Omega_0^I(s)^{-1}]$ can be replaced by $-\beta \mathrm{Re}\mathcal{T}_0^I(s)$ in order to compute the integral in Eq. (6).

After this consistency check, we next input *experimental* $\pi\pi$ phases, based on analyses of the CERN-Munich results by Ochs, by Estabrooks and Martin and by Hoogland et al. [22] extrapolated to threshold using the Roy equations (which are the partial wave projection of twice subtracted dispersion relations embodying full three channel crossing symmetry) for different values of the $I = 0$ S-wave $\pi\pi$ scattering length a_0^0. The complete details of these calculations are given in [6]. Figs. 5-7 show the predictions for the integrated $\gamma\gamma \to \pi^0\pi^0$ cross-section. Firstly, in Fig. 5 we have the curve "$EXP\pi$" with the

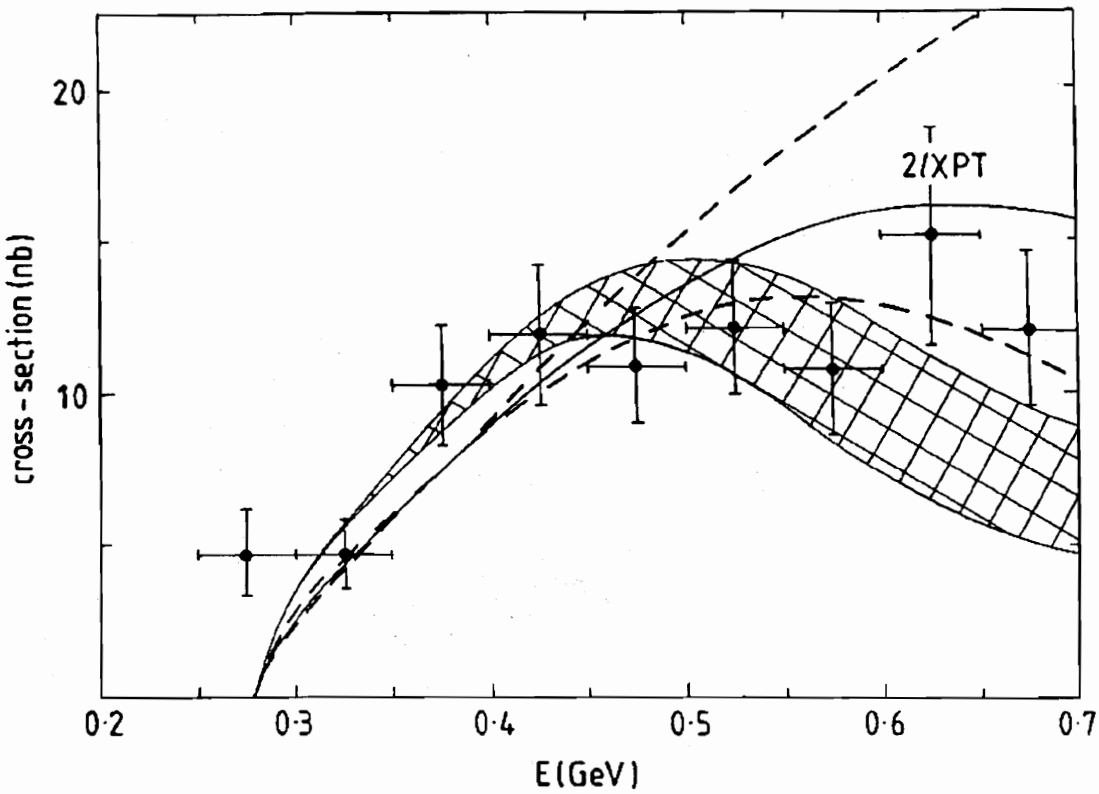

Figure 6: Integrated cross-section for $\gamma\gamma \to \pi^0\pi^0$ as a function of the $\pi\pi$ invariant mass, $E = \sqrt{s}$. The data are from Crystal Ball [3] scaled to the full angular range by a factor of 1.25. The band depicts our dispersive prediction using the central phases of Fig. 17 of Ref. 6 with $a_0^0 = 0.2$. The shaded area is a reflection of both the experimental uncertainty above 500 MeV in the S-wave $\pi\pi$ phases and the different asymptotics for the vector exchanges [6]. The band delineated by the dashed lines and the solid central curve marked $2\ell\chi PT$ is the prediction of 2 loop Chiral Perturbation Theory [24].

input of π exchange, experimental $\pi\pi$ phases with $a_0^0 = 0.2$ and $s_n = m_\pi^2$. This is already in better agreement with the near threshold data. In Fig. 6 we add, to the inputs of Fig. 5, ρ and ω exchanges. The values of the couplings of the various t and u-channel exchanges on-mass shell have been given by Ko [23] and are discussed in [6]. The addition of ρ, ω exchange brings an even better measure of agreement with experiment over a much larger energy range up to 500-600 MeV (as may have been anticipated from Fig. 3). In Fig. 6 we also show the band ($2\ell\chi$PT) given by the recently completed two loop calculation in χPT by Bellucci, Gasser and Sainio [24]. This is in good agreement with the dispersive results — the small discrepancy near threshold is due to a small difference in the $\pi\pi$ phases input into our calculation and those of χPT near threshold. The two loop calculation

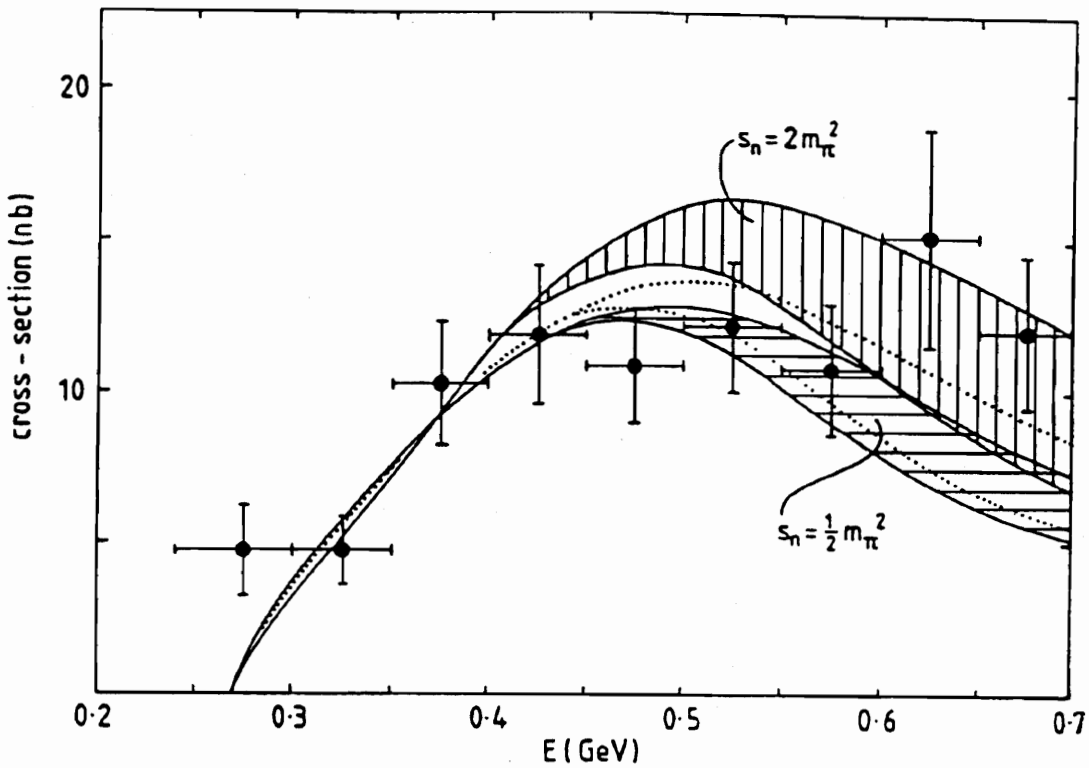

Figure 7: Integrated cross-section for $\gamma\gamma \to \pi^0\pi^0$ as a function of the $\pi\pi$ invariant mass, $E = \sqrt{s}$. The data are from Crystal Ball [10] scaled to the full angular range by a factor of 1.25. The three bands show the effect of varying the sub-threshold zero for $\gamma\gamma \to \pi^0\pi^0$ from $s_n = \frac{1}{2}m_\pi^2$ (the lower, horizontally shaded region) to m_π^2 (the unshaded region bounded by the dotted lines) to $2m_\pi^2$ (the higher, vertically shaded region). Again the bands mark the uncertainties in the calculations [6].

depends on a significant number of new constants, beyond the lowest order parameters f_π and m_π. These new constants have their analogue in the dispersive approach, Eq. (12), as we comment on later.

To have an idea of how much the dispersive predictions for $\gamma\gamma \to \pi\pi$ reflect our specific inputs, we illustrate the dependence on the position, s_n of the zero in the $\gamma\gamma \to \pi^0\pi^0$ S-wave and on the low energy $\pi\pi$ phases. Thus Fig. 7 shows the results with π, ρ, ω exchanges, $a_0^0 = 0.2$ and $s_n = \frac{1}{2}m_\pi^2$, m_π^2, $2m_\pi^2$ in turn, while Fig. 8 has the same left hand cut, but with $s_n = m_\pi^2$ and $a_0^0 = 0.1, 0.2, 0.3$. Of course, χPT has a definite view of what these parameters a_0^0 and s_n are. Figs. 6-8 illustrate how data on $\gamma\gamma \to \pi^0\pi^0$ can calibrate these predictions.

Fig. 9 shows the corresponding prediction from the present dispersive approach for $\gamma\gamma \to \pi^+\pi^-$, with the same inputs as for Fig. 8. Notice that in the charged channel,

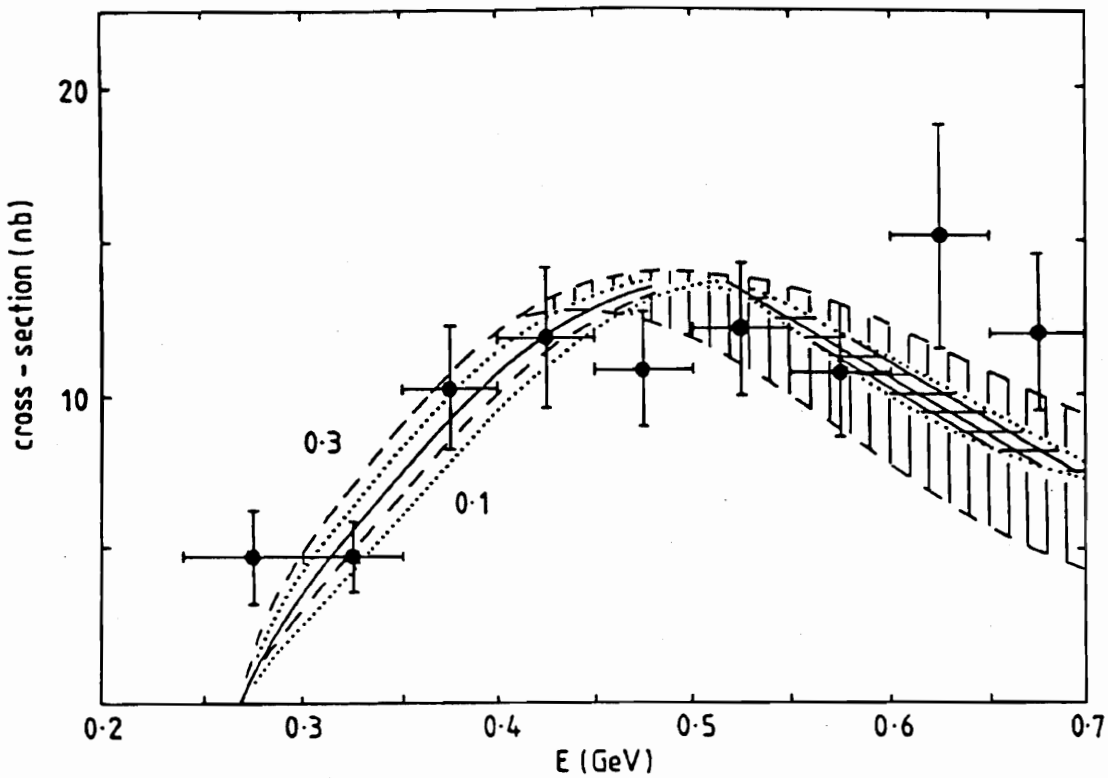

Figure 8: Integrated cross-section for $\gamma\gamma \to \pi^0\pi^0$ as a function of the $\pi\pi$ invariant mass, $E = \sqrt{s}$. The data are from Crystal Ball [10] scaled to the full angular range by a factor of 1.25. The lines, labelled by the value of the $I = 0$ $\pi\pi$ S-wave scattering length in steps of 0.05 from 0.1 to 0.3, illustrate the effect of different extrapolations of the $\pi\pi$ phases above 520 MeV down to threshold on the dispersive prediction [6]. The bands above 500 MeV on the $a_0^0 = 0.1$ and 0.3 curves mark the range generated by different asymptotics for the vector exchanges [6].

the effect of final state interactions is to enhance the Born cross-section very close to threshold and then suppress it above 360 MeV. One loop χPT for the charged channel only displays the near threshold enhancement. The two loop calculation presently under way may be expected to show the same suppression above 400 MeV, if it is to agree with this dispersive result and, of course, experiment. This will be an interesting test.

We see from Figs. 8,9 that our dispersive results mean that to determine the $\pi\pi$ scattering length a_0^0 to an accuracy of ± 0.1 requires the integrated $\gamma\gamma \to \pi\pi$ cross-section between 300 and 400 MeV to be measured to an accuracy of ± 20 nb in the $\pi^+\pi^-$ channel and ± 1.5 nb in the $\pi^0\pi^0$ mode. This should be quite possible at DAΦNE, but to achieve considerably greater accuracy seems less likely in the $\gamma\gamma$ channel. Rather these processes provide a consistency check on otherwise measured $\pi\pi$ phases and give a way of pinning

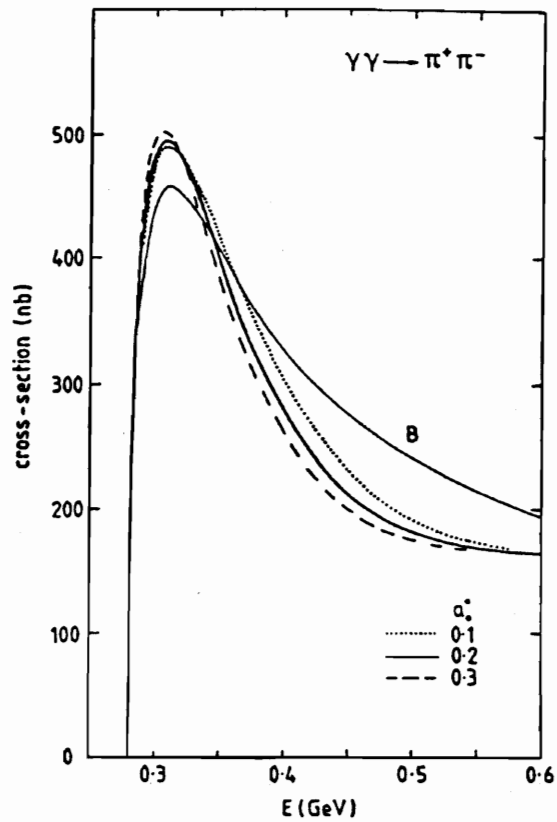

Figure 9: Dispersive predictions for the integrated cross-section for the $\gamma\gamma \to \pi^+\pi^-$ cross-section as a function of the $\pi\pi$ invariant mass, $E = \sqrt{s}$. The lines, labelled by the value of the $I = 0$ $\pi\pi$ S-wave scattering length in steps of 0.1 from 0.1 to 0.3, illustrate the effect of different extrapolations of $\pi\pi$ phases above 520 MeV down to threshold [6] (cf. Fig. 8). The curve marked B is the Born cross-section [1, 3].

down the slopes of the low energy amplitudes that fix the zero s_n, for example. Of course, χPT makes a definite statement about how far from m_π^2 the zero position, s_n, can be, but tests of this theory require us to analyse data without inputting this information. As seen from the predictions of Fig. 7, to do this very accurately looks a tall order. We will comment on the implications of this for the model-independent extraction of the pion polarizabilities in Sect. 4.

It is important to realise that the $\pi^+\pi^-$ and $\pi^0\pi^0$ cross-sections are strongly correlated. A 10% change in the charged data near threshold would mean a 100% change in the neutral cross-section. Thus early hints from the very small statistics experiment of DM1/2 [25] that the low energy $\gamma\gamma \to \pi^+\pi^-$ cross-section may be a factor of two larger than the Born cross-section would have required a $\gamma\gamma \to \pi^0\pi^0$ cross-section of 100 nb [4] rather than the ~10 nb seen by Crystal Ball (Fig. 4) near threshold. It is this close correlation

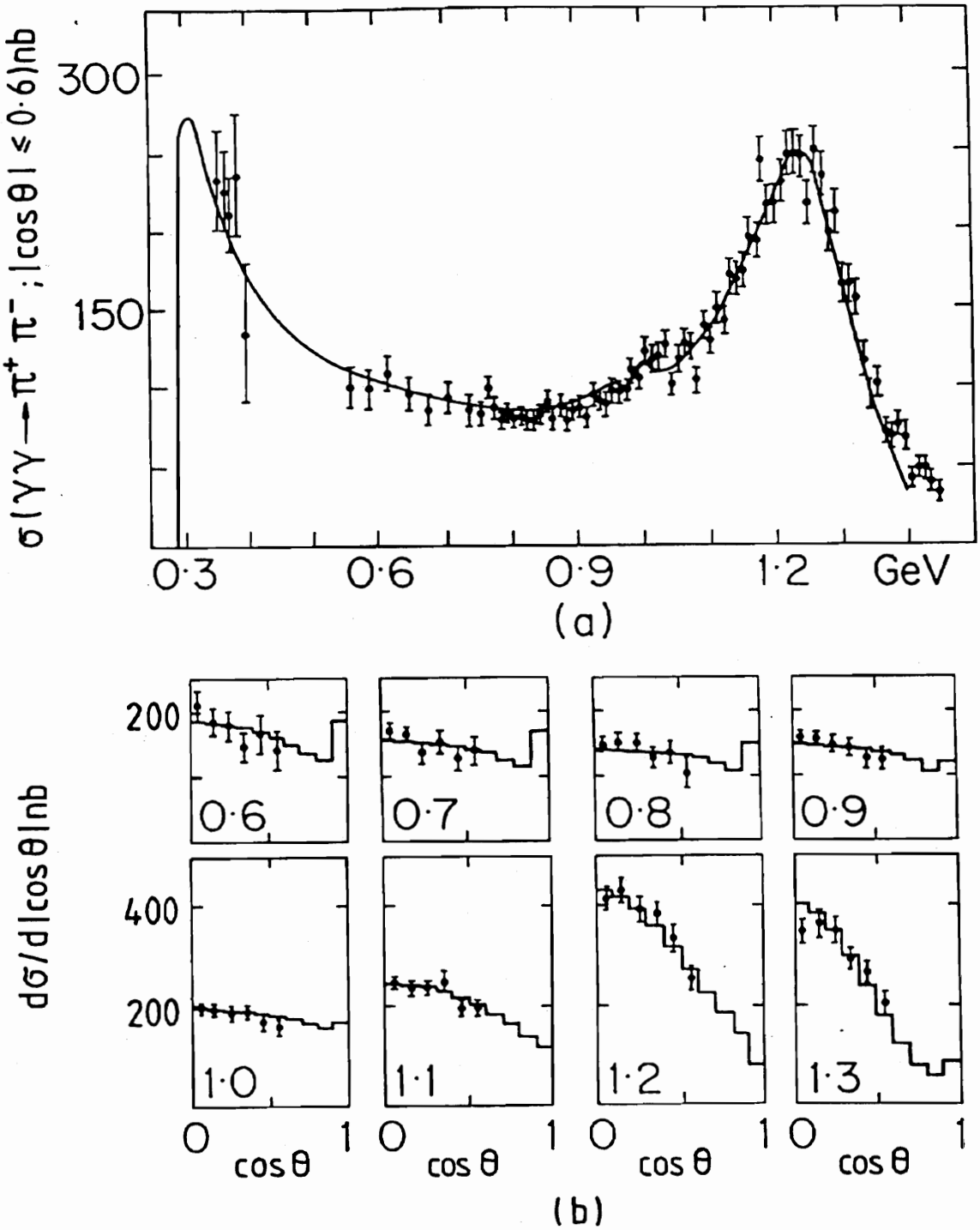

Figure 10: (a)Integrated cross-section for the $\gamma\gamma \to \pi^+\pi^-$ as a function of the $\pi\pi$ invariant mass, $E = \sqrt{s}$, from Mark II [7] ; (b) the corresponding differential cross-sections as a function of $\cos\theta$ in the stated mass bins (in units of GeV). The curves are the fits up to 1.4 GeV from the dispersive analysis of Ref. 11.

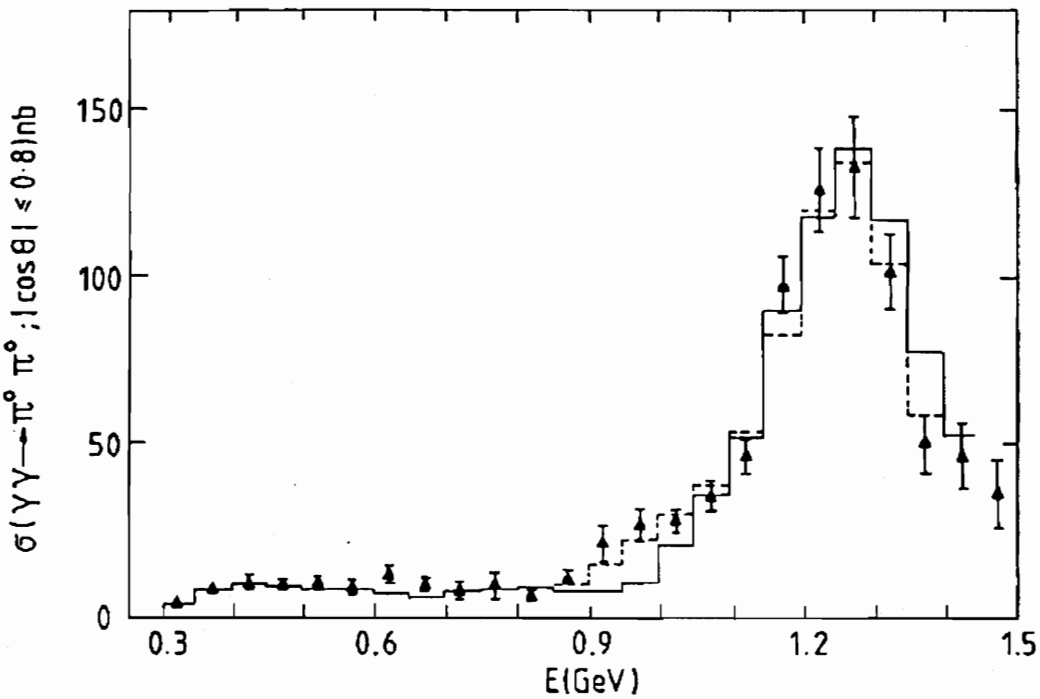

Figure 11: Integrated cross-section for the $\gamma\gamma \to \pi^0\pi^0$ as a function of the $\pi\pi$ invariant mass, $E = \sqrt{s}$, from Crystal Ball [10]. The histograms are from the dispersive analysis up to 1.4 GeV of Ref. 11. They show two fits with different $f_0(980) \to \gamma\gamma$ couplings.

and agreement between the Mark II and Crystal Ball data of Figs. 4,10,11 that is so reassuring. DAΦNE should be able to probe this further and allow a better low energy anchor for partial wave analyses at higher energies, to which we now turn.

The region of applicability of the dispersive predictions we have presented here is below 500 MeV or so. Above that details of cross-channel exchanges and inelastic phases become increasingly relevant. The representation of the $\gamma\gamma \to \pi\pi$ amplitude in terms of left hand cut effects becomes less and less economical as the various exchanges π, $\pi\pi$, $\pi\pi\pi$, ρ, ω, a_1, b_1, $\rho\rho$, $\rho\omega$, etc., crowd in towards the $\gamma\gamma \to \pi\pi$ physical region, Fig. 3. Instead a direct channel representation of the non-pion exchange effects becomes the most economical, as described above, Eq. (12) with $\mathcal{P}_C \neq 0$. Of course, the two descriptions are equivalent, but a single direct channel resonance is generated by an infinite number of cross-channel exchanges and the description of the former is clearly far more economical. Nevertheless, from 600 MeV to 2 GeV, the pion exchange Born term continues to play a significant role (Fig. 3) [3, 4].

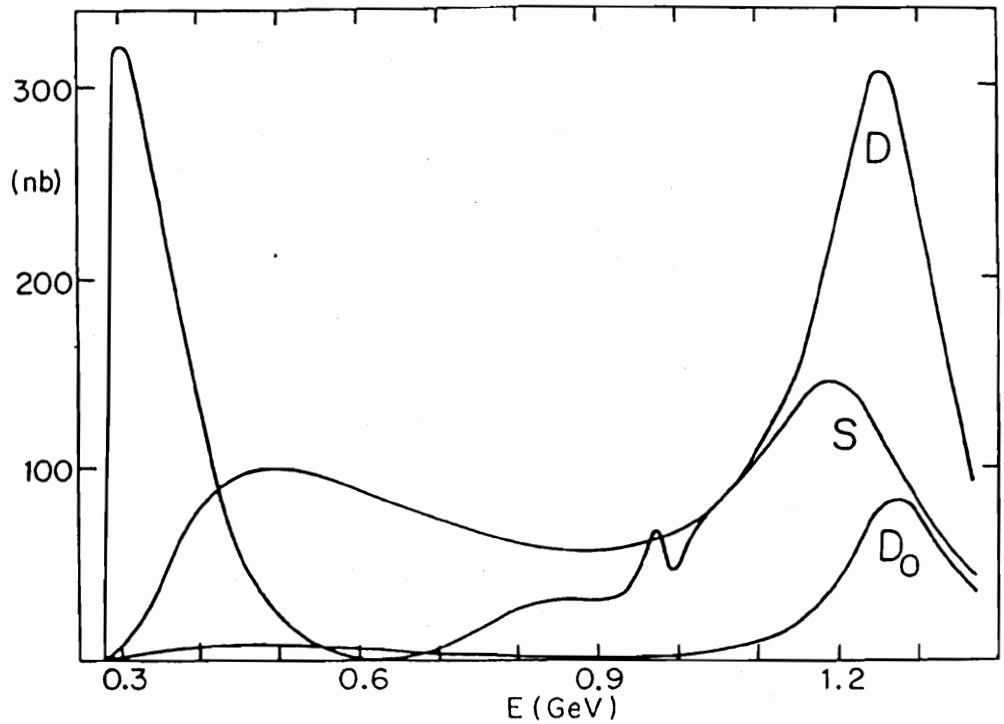

Figure 12: Typical integrated cross-sections for individual $I = 0$ partial wave components for $\gamma\gamma \to \pi\pi$ as a function of $\gamma\gamma$ c.m. energy from the Amplitude Analysis of the fits of Figs. 10,11 [11]. Notice that the S-wave is highly structured. The peak near threshold largely reflects the Born term. The dip at 600 MeV is caused by the effect of final state interactions on this Born term. These final state interactions are dominated by the broad $f_0/\epsilon(1000)$, which is seen up to 1300 MeV, on top of which is the narrow $f_0/S^*(980)$ signal. D denotes the total spin two component, i.e. the sum of helicity 0 and 2, while D_0 is just the helicity 0 part.

This is most readily illustrated for the D-wave, for which the helicity 2 component becomes rapidly important away from threshold. This partial wave exhibits the $f_2(1270)$ resonance, Figs. 4,10-12, which is known to be a highly elastic $\pi\pi$ resonance with a weak coupling to the $K\overline{K}$ channel [12], just as expected from ideal mixing. It is natural to assume that this partial wave in the $\gamma\gamma \to \pi\pi$ channel continues to have the same phase as in $\pi\pi \to \pi\pi$ above the inelastic threshold, indeed through the $f_2(1270)$ region up to 1.5 GeV, say. Then, the final state corrections to the Born amplitude are calculable, using Eqs. (10,12) with $h = \mathcal{B}^\pi$. As noted by Mennessier [14] and by Morgan and the present author [3] in this context and by Basdevant and Berger [26] in other related situations, this amplitude actually has a zero close to the resonance position, here near 1270 MeV.

Thus the modifications to the real pion exchange Born term necessary to make it agree with unitarity and have the phase of 90° at the f_2 mass, also place a zero there. In terms of Feynman diagrams, this means the graphs (a, b) of Fig. 13 do not contribute to the f_2-peak (though importantly they do affect its observed shape). Rather a direct $\gamma\gamma$ coupling of the $f_2(1270)$ is needed, Fig. 13c, or equivalently a sum of a large number of cross-channel exchanges. Thus, in accord with common sense, the $\gamma\gamma \rightarrow f_2(1270)$ coupling cannot be predicted, unless one knows all the cross-channel exchange couplings. Rather one must determine such resonance couplings from the measured cross-sections.

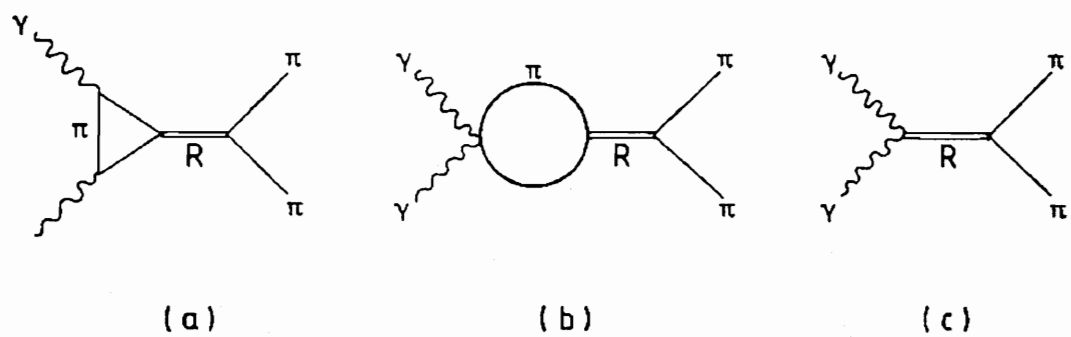

Figure 13: (a,b) Feynman diagrams displaying the contribution of final state scattering for the Born amplitude through a resonance, R, encoded in the $\mathcal{P}_B$ term of Eq. (11) ; (c) the direct coupling of the same resonance to $\gamma\gamma$ and $\pi\pi$ emobodied in the $\mathcal{P}_C$ term of Eq. (11).

An exactly analogous zero (seen in Fig. 12) occurs in the $I = 0$ S-wave Born amplitude, modified by final state interactions, at 600 MeV [3], as a result of the broad $\pi\pi$ enhancement, the $f_0/\epsilon(1000)/f_0(1300)$. Again simply adding Breit-Wigners to Born amplitudes fails to respect Watson's theorem and the above machinery is essential for any meaningful extraction of resonance couplings. Thus to go beyond about 500 MeV in describing $\gamma\gamma \rightarrow \pi\pi$ scattering, one must include direct $f_2(1270)$, $f_0/\epsilon(1000)$ and $f_0/S^*(980)$ couplings [3] in a way consistent with analyticity, Watson's theorem and Low's low energy theorem. Such an analysis was performed by David Morgan and myself [11] to the earlier Crystal Ball statistics on $\gamma\gamma \rightarrow \pi^0\pi^0$ [10] and Mark II results on $\gamma\gamma \rightarrow \pi^+\pi^-$ [7] and

[3]These coupling parameters also arise in two and higher loop χPT . For example, in the two loop calculation [24] the $\gamma\gamma$ couplings of the scalar and tensor resonances are included as well as the $\gamma\pi$ couplings of the vector and axial vector mesons and the usual Chiral Lagrangian parameters $\overline{\ell_i}$.

a new analysis was begun together with Karch [27], incorporating the increased Crystal Ball statistics above 800 MeV and the newer CELLO data [8] on the charged channel. In Figs. 10,11 are shown illustrative results (the corresponding plots for $\gamma\gamma \to \pi^0\pi^0$ angular distributions are to be seen in Ref. 11). One sees that the dispersive description fits the integrated and differential cross-sections up to 1400 MeV remarkably well. This allows a partial wave separation, the $I = 0$ components being shown in Fig. 12. This leads to the following couplings [11] for the $f_0(1000)$, $f_0(980)$ and $f_2(1270)$ (quoted in the PDG tables [12]) :

$$\begin{aligned} \Gamma(f_0/S^*(980)) \to \gamma\gamma) &= (0.63 \pm 0.14)\ \text{keV} \quad ; \\ \Gamma(f_0/\epsilon\ (1000)) \to \gamma\gamma) &= (5.4\ \pm 2.3\ )\ \text{keV} \quad ; \\ \Gamma(f_2(1270)) \to \gamma\gamma) &= (2.35 \pm 0.65)\ \text{keV} \quad . \end{aligned} \tag{15}$$

4. Polarizabilities

The polarizabilities — electric α, magnetic β — of a particle, like its charge radius, reflect its response to an electromagnetic stimulus [28, 21, 29]. They are related to how the Compton amplitudes approach the Born limit at threshold. Thus the combination $(\alpha - \beta)$ is determined by the slope of the S-wave $\gamma\gamma \to \pi\pi$ amplitude at the cross-channel threshold :

$$(\alpha - \beta) = \frac{4\epsilon\alpha}{m_\pi} \lim_{s\to 0} \frac{\mathcal{F}_{00}(s) - \mathcal{B}_{00}(s)}{s} \quad , \tag{16}$$

where for the charged pion case $\mathcal{B}$ is the one-pion-exchange Born amplitude, $\mathcal{B}^\pi$, $\epsilon = 1$, and for neutral pions $\mathcal{B} = 0$, $\epsilon = -1$ with our definition of Eq. (4). In terms of the dispersive representation of Eqs. (6-9), these polarizabilities are simply related to the subtraction constants [6] and, of course, the ρ, ω exchange contributions at $s = 0$:

$$\begin{aligned} (\alpha - \beta)_c &= \frac{4\alpha}{m_\pi}\left[\sqrt{\frac{2}{3}}\, d_0 + \sqrt{\frac{1}{3}}\, d_2 - \sqrt{\frac{2}{3}}\, \mathcal{L}^{\rho\prime}(0)\right] \quad , \\ (\alpha - \beta)_n &= \frac{4\alpha}{m_\pi}\left[\sqrt{\frac{1}{3}}\, d_0 - \sqrt{\frac{2}{3}}\, d_2 + \sqrt{\frac{1}{3}}\, \mathcal{L}^{\rho\prime}(0) - \mathcal{L}^{\omega\prime}(0)\right] \quad . \end{aligned} \tag{17}$$

Moreover, these combinations are sensitively related to the position of any sub-threshold zeros. In the neighbourhood of $s = 0$, the charged and neutral S-wave amplitudes can be

parametrized as

$$\mathcal{F}^c \simeq \mathcal{B}^\pi + b_c\, s(s_c - s) \quad , \quad \mathcal{F}^n \simeq b_n\, s(s - s_n) \quad , \tag{18}$$

then

$$(\alpha - \beta)_c = b_c s_c \quad , \quad (\alpha - \beta)_n = b_n s_n \quad . \tag{19}$$

Note that this approximation is only valid for $0 \leq s \ll 4m_\pi^2$, since the amplitudes have a cusp at $\pi\pi$ threshold, which is particularly marked in the $\pi^0\pi^0$ amplitude, see Fig. 25 of Ref. 6 or Fig. 8 of Bellucci et al. [24] in 2 loop standard χPT or Fig. 6 of Knecht et al. [30] in 1 loop generalized χPT . Of course χPT has a definite expectation for the values of s_c and s_n. However, we have seen from Fig. 7 that present (or even future) data cannot tell without a model parametrization whether the sub-threshold zero in the neutral channel is at $s_n = m_\pi^2/2$, m_π^2 or $2m_\pi^2$. This variation leads to a factor of four difference in the neutral polarizability $(\alpha - \beta)_n$ from -0.6 to -2.7×10^{-43} cm^3. These values are merely illustrative [4], in practice the range of uncertainty of a model-independent extraction is still larger. Moreover, present data even allow s_c to be zero, so $(\alpha - \beta)_c$ could be zero, also with a very large uncertainty.

Rather than use the sub-threshold behaviour around $s = m_\pi^2$ as we have done in Sect. 3 to fix the $S-$wave subtraction constants, d_I, Kaloshin and Serebryakov [31] have attempted a closely related dispersive analysis in which the subtraction constants for the S-wave are parametrized directly in terms of the polarizabilities $(\alpha - \beta)_{c,n}$. They find in units of 10^{-43} cm^3 : $(\alpha - \beta)_c = (5.3 \pm 1.0)$; $(\alpha - \beta)_n = (0.6 \pm 1.8)$. As just remarked a value of $(\alpha - \beta)_c = 0$ is perfectly consistent with the charged channel data, so why have Kaloshin and Serebryakov [31] excluded this by many standard deviations ? This is because though they only fit the Mark II $\gamma\gamma \to \pi^+\pi^-$ data [7] below 400 MeV, they include in their fit data on $\gamma\gamma \to \pi^0\pi^0$ [10] up to 850 MeV and yet assume they know the form of all the cross-channel exchanges π, ρ, ω very far from their t and u-channel poles. The existence of the $f_0/\epsilon(1000)$ and $f_0/S^*(980)$, the former markedly affects data at 800 MeV, because of its large width (Fig. 12), require many more exchanges than ρ and ω. Moreover, even in going from the ρ and ω poles at $t = m_V^2$, where the couplings are, of course, determined by the measured $V \to \pi\gamma$ rates, to the Compton threshold at $t = m_\pi^2$, the couplings can change by a factor of 2 — a simple Veneziano-like model with towers of resonances, not just the ρ and ω gives a factor of $\pi/2$ [5]. To then assume at 850 MeV, where $-m_V^2 \lesssim t, u \leq 0$, the pure ρ and ω exchange amplitudes have the same couplings

[4] note that the values quoted in Ref. 6 are for $\mid \alpha - \beta \mid_n$ and are in different units.

[5] thereby dramatically affecting their contributions to Eq. (6) of Ref. 31.

as at $t, u = +m_V^2$ is a grossly over-simplified model leading to far too small an estimate of the uncertainties on the supposedly determined polarizabilities. That the details of the cross-channel exchanges become increasingly important at higher $\pi\pi$ masses can be seen from Fig. 3 and from the band shown in Fig. 6.

We now turn to the determination of $(\alpha + \beta)$ combinations of polarizabilities. While the $(\alpha - \beta)_{c,n}$ are related to how the $\gamma\gamma \to \pi\pi$ S-waves approach their Born term as $s \to 0$, Eq. (16), the $(\alpha + \beta)_{c,n}$ are determined by the way the helicity two D-waves approach their Born term at the same Compton threshold. These are even more difficult to determine from $\gamma\gamma \to \pi\pi$ data. As we have stressed, it is only in the very low energy region that cross-channel exchange contributions are accurately calculable. Below 500 MeV, the D-wave amplitude is overwhelmingly ($\sim$ 99%) controlled by its Born component. It is the residual $\sim$ 1% that has to be extrapolated to $s = 0$ to determine the $(\alpha + \beta)$ combinations of polarizabilities, clearly an impossible task with present data that only cover a very limited part of the angular range. More accurate separation of higher waves with helicity two will become possible using the azimuthal information that the DAΦNE $\gamma\gamma$ experiment should provide [32, 33, 34]. However, this has not deterred Kaloshin, Persikov and Serebryakov [35] from attempting a *first estimate* of the $(\alpha + \beta)$ with amazing results. They have once again, even up to 1.4 GeV in $\pi\pi$ mass, assumed only elementary π, ρ and ω exchange determine the left hand cut effects. No obvious t, u-dependence is included in the pole numerators, even though t, u-channel unitarity demand these. They then add an $f_2(1270)$ direct channel contribution assuming this to be wholly helicity two with no S-wave background under this. While present data are not incompatible with this, they are equally consistent (see Fig. 12) with 30% of the $I = 0$ cross-section from 1–1.4 GeV being S-wave [11, 8] and possibly 30% of the D-wave having helicity zero [11]. This provides at least a 40–50% uncertainty in the f_2-contribution to the helicity two D-wave cross-section. Yet Kaloshin et al. [35] quote values of $(\alpha + \beta)_n$ with 5% errors : $(\alpha + \beta)_n = (1.00 \pm 0.05)$, far away at $s = 0$.

In the dispersive treatment discussed above, the description of the $f_2(1270)$ region in terms of Eq. (12), $\Omega^I_{J,\lambda}(s)$ embodies the expected Breit-Wigner shape of the resonance, while $\mathcal{P}_C(s)$ provides a smooth modulation of this over the peak in much the same way as the ρ-line shape in $e^+e^- \to \pi^+\pi^-$ differs smoothly from that in $\pi\pi$ elastic scattering. The exact form of $\mathcal{P}_C(s)$ depends, of course, on the structure of the left hand cut discontinuity embodied in the model for $\mathcal{H}^I_{J,\lambda}(s)$ defining $\mathcal{P}_C$ in Eq. (12). Kaloshin et al. take their analogue of $\mathcal{P}_C(s)$ to be a constant, as far as its s-dependence is concerned. However, $\mathcal{P}_C(s)$ is really built from many t and u-channel exchanges. While these do generate a

smooth form over the f_2-region from 1 to 1.4 GeV, for almost any couplings, it is the exact values of these individually that determines the extrapolation to $s = 0$ (cf. the analogue of Eq. (17)). Consequently, the analysis of Kaloshin, Persikov and Serebryakov [35] is misguided. Fitting in the f_2-region can in no way determine the polarizability $(\alpha + \beta)$ charged or neutral. This is obvious from the structure of Fig. 3, where exchanges crowd in near the physical region and only their collective effect is measured, whereas in extrapolating to $s = 0$, it is the individual exchange contributions that matter.

All this means that the only way to measure the pion polarizabilities is in the Compton scattering process near threshold and not in $\gamma\gamma \to \pi\pi$. Though low energy $\gamma\gamma \to \pi\pi$ scattering is seemingly close to the Compton threshold ($\sqrt{s} \geq 2m_\pi$ to $\sqrt{s} = 0$) and so the *extrapolation* not very far, the dominance of the pion pole (for final state interaction effects, for example) means that the energy scale for this continuation is m_π. Thus the polarizabilities cannot be determined accurately from $\gamma\gamma$ experiments in a model-independent way and must be measured in the Compton scattering region [29].

5. Summary

Measurements of $\gamma\gamma \to \pi\pi$ scattering at DAΦNE will fulfill a number of aims :

(a) they will test the predictions of χPT ,

(b) they will fix the sub-threshold zero in the $\gamma\gamma \to \pi^0\pi^0$ channel,

(c) they will provide an independent check of low energy $\pi\pi$ phases, and

(d) they will anchor partial wave analyses of data at higher $\pi\pi$ masses, and so allow a better determination of the couplings of the scalars $f_0/S^*(980)$ and $f_0/\epsilon(1000)$ so crucial for understanding their quark composition [11, 36].

For all these, measurements of the angular distributions over as complete a coverage as possible is vital [33, 37]. We have much to learn.

To conclude : the importance of measuring $\gamma\gamma \to \pi\pi$ scattering at DAΦNE should not be underestimated. Consequently, we eagerly await the precision measurements of the KLOE detector at DAΦNE.

It is a pleasure to thank Rinaldo Baldini, Stefano Bellucci, André Courau, Jürg Gasser, David Morgan and Jorge Portolés for numerous invaluable discussions.

References

[1] S.J. Brodsky, T. Kinoshita and H. Terazawa, Phys. Rev. D4 (1971) 1532 ;
V.M. Budnev, I.F. Ginsburg, G.V. Meledin and V.G. Serbo, Phys. Rep. 15C (1975) 181 ;
M. Poppe, Int. Journ. Mod. Phys. A1 (1986) 545 ;
Ch. Berger and W. Wagner, Phys. Rep. 146C (1987) 1 ;
H. Kolanoski and P. Zerwas in "High energy electron-positron physics", ed. A.Ali and P. Söding (World Scientific, 1988) ;
S. Cooper, Ann Rev. Nucl & Part. Phys. 38 (1988) 705 ;
D.Morgan, M.R. Pennington and M.R. Whalley, J.Phys. G20 (Supp. 8A) (1994) A1.

[2] F.E. Low, Phys. Rev. 96 (1954) 1428 ;
M. Gell-Mann and M.L. Goldberger, Phys. Rev. 96 (1954) 1433 ;
H.D.I. Abarbanel and M. Goldberger, Phys. Rev. 96 (1968) 1594.

[3] D. Morgan and M.R. Pennington, Phys. Lett. 192B (1987) 207 , Z. Phys. C37 (1988) 431, Z. Phys. C39 (1988) 590.

[4] M.R. Pennington, Proc. VIII International Workshop on photon-photon collisions, Shoresh, Israel, 1988, ed. U. Karshon (World Scientific, 1988) pp. 297-325.

[5] DAΦNE Physics Handbook, ed. L. Maiani, G. Pancheri and N. Paver (INFN, Frascati, 1992).

[6] M.R. Pennington in [5], p. 379.

[7] J. Boyer et al. (Mark II Collab.), Phys. Rev. D42 (1990) 1350.

[8] H.J. Behrend et al. (CELLO Collab.), Z. Phys. C56 (1992) 381.

[9] Ch. Berger et al. (PLUTO Collab.), Z. Phys. C26 (1984) 199.

[10] H. Marsiske et al. (Crystal Ball/DORIS Collab.), Phys. Rev. D41 (1990) 3324.

[11] D. Morgan and M.R. Pennington, Z. Phys. C48 (1990) 623.

[12] Particle Data Group, *Review of Particle Properties*, Phys. Rev. D50 (1994) 1173.

[13] D.H. Lyth, Nucl. Phys. B30 (1971) 195, Nucl. Phys. B48 (1972) 537 ; J. Phys. G10 (1984) 39, J. Phys. G10 (1984) 1777.

[14] G. Mennessier, Z. Phys. C16 (1983) 241 ;
G. Mennessier and T.N. Truong, Phys. Lett. 177B (1986) 195.

[15] K.M. Watson, Phys. Rev. 88 (1952) 1163.

[16] R. Omnès, Nuovo Cim. 8 (1958) 316.

[17] D. Morgan and M.R. Pennington, Phys. Lett. B272 (1991) 134.

[18] J. Bijnens and F. Cornet, Nucl. Phys. B296 (1988) 557.

[19] J.F. Donoghue, B.R. Holstein and Y.C. Lin, Phys. Rev. D37 (1988) 2423.

[20] S. Weinberg, Phys. Rev. Lett. 17 (1966) 616.

[21] J.F. Donoghue and B.R. Holstein, Phys. Rev D48 (1993) 137.

[22] W. Ochs, Univ. of Munich thesis, 1974 ;
P. Estabrooks and A.D. Martin, Nucl. Phys. B79 (1974) 301 ;
W. Hoogland et al., Nucl. Phys. B126 (1977) 109.

[23] P. Ko, Phys. Rev D41 (1990) 1531.

[24] S. Bellucci, J. Gasser and M.E. Sainio, Nucl. Phys. B423 (1994) 80.

[25] A. Courau et al. (DM1 Collab.), Nucl. Phys. B271 (1986) 1 ;
Z. Ajaltouni et al. (DM2 Collab.), Phys. Lett. B194 (1987) 573.

[26] J-L. Basdevant and E.L. Berger, Phys. Rev. D16 (1977) 657.

[27] K. Karch, D. Morgan and M.R. Pennington (unpublished work, 1991).

[28] B.R. Holstein, Comm. Nucl Part. Phys. 20 (1992) 301.

[29] J. Portolés and M.R. Pennington, contribution to the Second DAΦNE Physics Handbook, eds. G. Pancheri and N. Paver (INFN, Frascati, 1995)(to be published).

[30] M. Knecht, B.Moussallam and J. Stern, Nucl. Phys. B429 (1994) 125.

[31] A.E. Kaloshin and V.V. Serebryakov, Z. Phys. C (to be published).

[32] P. Kessler and S. Ong, Mod. Phys. Lett. A2 (1987) 683 ; Phys. Rev. D46 (1992) 944.

[33] G. Alexander et al., Frascati preprint LNF-93/030 (1993).

[34] A. Courau and S. Ong, verbal contributions to the Working Group on DAΦNE Physics.

[35] A.E. Kaloshin, V.M. Persikov and V.V. Serebryakov, Irkutsk preprint ISU-IAP-TH-94-01.

[36] T. Barnes, Proc. VII Int. Workshop on photon-photon collisions, Paris, 1986, ed. A. Courau ; Phys. Lett. 165B (1985) 434 ;
N.N. Achasov and V.N. Ivanchenko, Nucl. Phys. B315 (1989) 465 ;
F.E. Close, Proc. Workshop on Physics and Detectors for DAΦNE, Frascati, April 1991, ed. G. Pancheri (INFN, Frascati) pp. 309-313 ;
M.R. Pennington, Proc. of meeting on Two-Photon Physics from DAΦNE to LEP200 and Beyond, Paris (Feb., 1994) ed. F. Kapusta and J. Parisi (to be published).

[37] F. Anulli et al., "The KLOE small angle tagging system at DAΦNE", Second DAΦNE Physics Handbook, eds. G. Pancheri and N. Paver (INFN, Frascati, 1995) (to be published).